Analytical Methods

ROYAL SOCIETY OF CHEMISTRY

PAPER

View Article Online
View Journal | View Issue

Cite this: *Anal. Methods*, 2022, **14**, 1956

An electrochemical biosensor based on few-layer MoS_2 nanosheets for highly sensitive detection of tumor marker ctDNA†

Zhilian Cui,[ab] Dujuan Li,[*ab] Weihuang Yang,[ab] Kai Fan,[c] Hongying Liu,[c] Fei Wen,[ab] Lili Li,[ab] Linxi Dong,[ab] Gaofeng Wang[ab] and Wei Wu[ab]

Received 18th March 2022
Accepted 2nd May 2022

DOI: 10.1039/d2ay00467d

rsc.li/methods

An electrochemical biosensor based on few-layer molybdenum disulfide (MoS_2) nanosheets was fabricated for the highly sensitive detection of tumor marker circulating tumor DNA (ctDNA) in this paper. The MoS_2 nanosheets with few layers were prepared by the shear stripping. Compared with the mechanical stripping method and the lithium ion intercalation method, this method is simpler to operate, and the prepared MoS_2 nanosheets had good electrochemical activity. The biosensing platform was fabricated based on the discriminative affinity of MoS_2 nanosheets towards single-stranded DNA (ssDNA) and double-stranded DNA (dsDNA). Methylene blue (MB) was used as the signal molecule. The results showed that the detection of ctDNA by this sensor showed an excellent linear relationship in the concentration range of 1.0×10^{-7} M to 1.0×10^{-16} M, and the detection limit was 2.5×10^{-18} M. In addition, this sensor exhibited outstanding stability and specificity. This strategy provides an alternative approach for ctDNA detection and an effective sensing strategy for future *in vitro* cancer diagnosis by label-free detection.

1 Introduction

Cancer is a life-threatening disease that is difficult to diagnose in the early stage and difficult to cure in the late stage. ctDNA is a nucleic acid fragment released by tumor cells into peripheral blood, and its quantity can effectively reflect tumor burden in the human body.[1] Because it carries tumor-associated alterations such as point mutations and DNA methylation,[2] ctDNA has been recognized as a promising biomarker for cancer diagnosis and monitoring. More importantly, the short half-life of ctDNA in peripheral blood, ranging from 2 hours to 1 day,[3] holds promise for real-time dynamic monitoring of chronic tumor changes and treatment response.[4] Therefore, there is an urgent need for a highly sensitive technique for detecting ultra-low concentrations of target ctDNA in the early stage of cancer.[5]

Among ctDNA nucleic acid sequences, E542K,[6] as a common mutation hotspot of PIK3CA,[7] exists widely in breast cancer, lung cancer, gastric cancer, liver cancer, colon cancer and brain cancer.[8–10] Therefore, the development of an efficient PIK3CA E542K ctDNA detection technology is of great significance for the diagnosis, prognosis and targeted therapy of tumors. Nowadays, many methods have been proposed to detect ctDNA, such as toehold-mediated strand displacement reaction (TSDR),[11] local surface plasmon resonance (LSPR),[12] polymerase chain reaction (PCR)[13] and DNA sequencing. However, there are still some problems in the detection technology of ctDNA, such as expensive equipment, complex biological functionalization means and insufficient target detection limit.[14]

In order to solve the above limitations, MoS_2 has attracted the attention of researchers. MoS_2 is a kind of transition metal sulfides constructed by stacking covalently bound S–Mo–S through weak van der Waals interactions,[15] which is one of the most concerned two-dimensional nano materials. MoS_2 nanosheets exhibit outstanding characteristics, such as the large specific surface area, the unique optical properties, and excellent electrical activities.[16] In addition, the interaction between MoS_2 and DNA provides a strategy for DNA detection. The principle of this strategy is that ssDNA can be adsorbed onto the MoS_2 nanosheets *via* van der Waals interaction, while dsDNA shows weaker interaction with MoS_2 nanosheets due to its rigid structure.[17,18] This finding has encouraged many researchers to develop different analytical strategies to detect DNA.[19–27]

Zhu *et al.*[28] proposed a nucleic acid sequence detecting method using the single-layer MoS_2 nanosheet as sensing platform. In this strategy, the fluorescence was quenched when the fluorescently-labeled ssDNA was adsorbed on the MoS_2 nanosheet *via* the van der Waals force. However, when the fluorescently-labeled ssDNA was hybridized with its complementary DNA, dsDNA could fall off the surface of MoS_2

[a]*Ministry of Education Engineering Research Center of Smart Microsensors and Microsystems, Hangzhou Dianzi University, Hangzhou, 310018, China. E-mail: dujuanli@hdu.edu.cn*

[b]*School of Electronics and Information, Hangzhou Dianzi University, Hangzhou, 310018, China*

[c]*School of Automation, Hangzhou Dianzi University, Hangzhou, 310018, China*

† Electronic supplementary information (ESI) available. See https://doi.org/10.1039/d2ay00467d

nanosheet, resulting in regeneration of the fluorescence. Li *et al.*[18] reported a label-free bioassay for DNA detection based on the size-dependent optical absorption of layered MoS_2 nanosheets. In the case of high salt concentration, layered MoS_2 nanosheets tended to aggregate rapidly, resulting in the increases of sizes in both vertical and lateral dimensions of the MoS_2 nanosheets, which was the result of the interplay between van der Waals attraction and electric double-layer repulsion.[17] When ssDNA was adsorbed on the layered MoS_2 nanosheets, the dispersion of MoS_2 nanosheets could produce great dispersion even in the presence of high concentration of salt, while the dispersion behavior weakened when ssDNA hybridized to form dsDNA. In addition, some composite materials based on MoS_2 nanosheets have also been developed.[29] For example, Zhang *et al.*[3] developed a high-performance sensing platform based on poly-xanthurenic acid (PXA) film functionalized MoS_2 nanosheets for detection of DNA in peripheral blood. Chu *et al.*[30] reported highly sensitive electrochemical detection of ctDNA based on thin-layer MoS_2/graphene composites. However, the mentioned above sensor technologies still face challenges such as high cost biomarkers, poor stability, complex material preparation, and long detection time.[31,32]

Herein, a DNA electrochemical sensor was fabricated based on few-layer MoS_2 nanosheets prepared by shear stripping to achieve the label-free and highly sensitive detection of the tumor marker ctDNA. The working principle of the fabricated DNA electrochemical sensor is shown in Fig. 1. Primarily, few-layer MoS_2 nanosheets with good electrochemical activity are modified onto the surface of the working electrode. After that, cpDNA is adsorbed on the modified surface of the working electrode through the special affinity between ssDNA and MoS_2 nanosheets. Then MB is used as the signal molecule,[15] based on the affinity between MB and DNA, resulting in the increase of electrochemical signal of MB on the surface of electrode. However, the dsDNA on the working electrode surface fall off by negative potential due to the weak affinity between dsDNA and MoS_2 nanosheets after hybridization of cpDNA and ctDNA, resulting in the decline of electrochemical signal of MB on the surface of electrode. Highly sensitive detection of DNA fixation and hybridization on the working electrode surface can be achieved based on the change of electrochemical signal of MB. This strategy is label-free and does not require signal amplification, which greatly reduces the operation steps and detection costs, and provides a new choice for ctDNA detection and analysis.

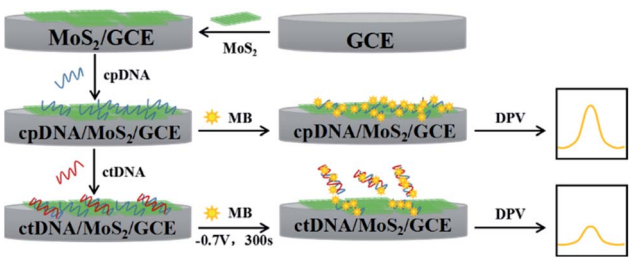

Fig. 1 Schematic diagram of the electrochemical biosensor based on the few-layer MoS_2 nanosheets.

2 Experimental section

2.1 Materials

MoS_2 powder (69860) and sodium cholate hydrate (≥99%, C1254) were purchased from Sigma-Aldrich, USA. Methylene blue (MB, M812933), sodium dodecyl sulfate (SDS, S885889) and anhydrous ethanol (99.5%) were all purchased from Shanghai MacLean Biochemical Technology Co. Ltd, China. PBS buffer (1× PBS, pH 7.2–7.4), Tris–HCl buffer (pH 7.4), SSC buffer and KCl were purchased from Shanghai Aladdin Biochemical Technology Co. Ltd, China. $K_3[Fe(CN)_6]$ was purchased from Sinopharm Chemical Reagent Co. Ltd, China. All DNA oligonucleotides were synthesized by Shanghai Sangong Biotechnology Co. Ltd, China. The sequences of these DNA are listed in Table 1.

All the chemical reagents were of analytical grade. Deionized water (Hangzhou Huake Water Treatment Equipment Co. Ltd, China) was used throughout the experiment.

2.2 Preparation and characterization of few-layer MoS_2 nanosheets

The few-layer MoS_2 nanosheets were prepared by a kitchen agitator (JB3060, Braun Inc., Germany). The resulting few-layer MoS_2 nanosheets was characterized by base field emission scanning electron microscope (Sigma 300, ZEISS, Germany) and atomic force microscope (Dimension Icon, Brock, Germany).

A mixed water solution, containing 50 mg mL^{-1} MoS_2 powder and 10 mg mL^{-1} sodium cholate hydrate, was mixed for 90 min at room temperature to prepare the few-layer MoS_2 nanosheets dispersion. To avoid overheating of both motor and liquid, a duty cycle of 2 min ON/2 min OFF was applied. The obtained suspension was centrifuged at 1500 rpm for 90 min. The top 50% liquid was collected, while the sediment was discarded to remove the unexfoliated bulk MoS_2. To remove extra sodium cholate in the solution, the supernatant was centrifuged

Table 1 DNA oligonucleotide sequences

DNAs	Sequences
Capture probe DNA (cpDNA)	5′-AGTGATTTTAGAGAG-3′
Complementary DNA (ctDNA)	5′-CTCTCTAAAATCACT-3′
One-base mismatched DNA (1 MT ctDNA)	5′-CTCTCTGAAATCACT-3′
Three-base mismatched DNA (2 MT ctDNA)	5′-CTCTCTGAAATGACG-3′
Non-complementary DNA (nc ctDNA)	5′-TAGAGCGCGCGATAG-3′

at 12 000 rpm for 20 min in order to isolate uniform layered dispersion MoS_2 nanosheets, and the collected sediment was then redispersed in deionized water. This washing process was repeated a further two times. Finally, the obtained sediment was dispersed in deionized water to prepare uniform layered dispersion. The stock solution of few-layer MoS_2 nanosheets should be used after 5 min of sonication.

2.3 Preparation of the modified electrodes

Bare electrodes need to be polished before use to reduce experimental errors caused by adsorbed impurities on the electrode surface. Suspension droplets of 20 μL few-layer MoS_2 nanosheets were dripped on the polished glassy carbon electrode (GCE) surface and dried naturally in the air. The obtained electrode was denoted as MoS_2/GCE. For comparison, bulk MoS_2 modified GCE electrode was also prepared, denoted as bulk MoS_2/GCE.

2.4 Immobilization and hybridization

2.4.1 DNA immobilization. 20 μL 1.0 μM cpDNA was dropped onto the MoS_2/GCE surface, and natural dried in the air. The electrode was cleaned with deionized water to remove the unfixed cpDNA and denoted as cpDNA/MoS_2/GCE. The cpDNA solution was prepared in 25 mM Tris–HCl buffer solution, pH 7.4.

2.4.2 DNA hybridization. Different concentrations of ctDNA (20 μL) were dropped onto the electrode surface of cpDNA/MoS_2/GCE, and then the ctDNA hybridized with the cpDNA. After naturally dried in the air, the electrodes were kept at −0.7 V for 300 s to release the dsDNA from the electrode surfaces.[33] The electrodes were thoroughly washed with 0.2% SDS solution before measurements. The ctDNA was prepared in 2× SSC buffer solution, pH 7.0.

2.5 Electrochemical measurements

Electrochemical measurements were performed with a Palmsens4 electrochemical workstation (PalmSens **https://www.instrument.com.cn/zc/473.html?AgentSortId=1474**, Holland) with a conventional three-electrode cell (Tianjin Aida Hengsheng Technology Development Co. Ltd, China). A three-electrode system was utilized. The bare or modified GCE was used as working electrode; a platinum wire was used as counter electrode, and an Ag/AgCl electrode was used as reference electrode. The cyclic voltammograms (CVs) were recorded in 1.0 M KCl solution containing 1.0 mM $[Fe(CN)_6]^{3-/4-}$. The potential was scanned from 0.6 V to −0.3 V with a scan rate of 100 mV s^{-1}. The electrochemical signals of MB were detected by differential pulse voltammetry (DPV). The pulse amplitude, pulse width, and pulse period were set as 0.05 V, 0.06 s and 0.2 s, respectively. Primarily, the working electrodes were immersed into the MB solution for 10 min. Then, the electrochemical signals of MB were measured in PBS buffer solution. In order to obtain reliable signals, the working electrodes were scanned for 10 cycles of voltammetry, followed by signal acquisition using DPV.

3 Results and discussion

3.1 Morphology characterizations of few-layer MoS_2 nanosheets

The liquid-based direct exfoliation has been regarded as a promising method for the preparation of MoS_2 nanosheets due to its advantages of scalable production, strong commonality and convenient operation.[17,34–37] In this study, few-layer MoS_2 nanosheets were obtained by shear stripping in sodium cholic acid aqueous solution using a kitchen blender that first proposed by Varrla *et al.*[38]

As is shown in Fig. 2(a), the few-layer MoS_2 nanosheets aqueous dispersion appears to be yellow-green in color. Fig. 2(b) shows the XRD patterns of MoS_2. All the identified peaks can be perfectly indexed to the standard pattern of the hexagonal MoS_2 (JCPDS card no. 37-1492). It can be seen from Fig. 2(b) that some diffraction peaks of few-layer MoS_2 nanosheets become weaker (for example, plane (002), (100), and (103)) and some diffraction peaks disappear (for example, plane (004), (102), and (106)) compared with bulk MoS_2.[22] The results showed that the number of MoS_2 layers decreased obviously after exfoliation. SEM was used to analyze the morphology of the bulk MoS_2 and

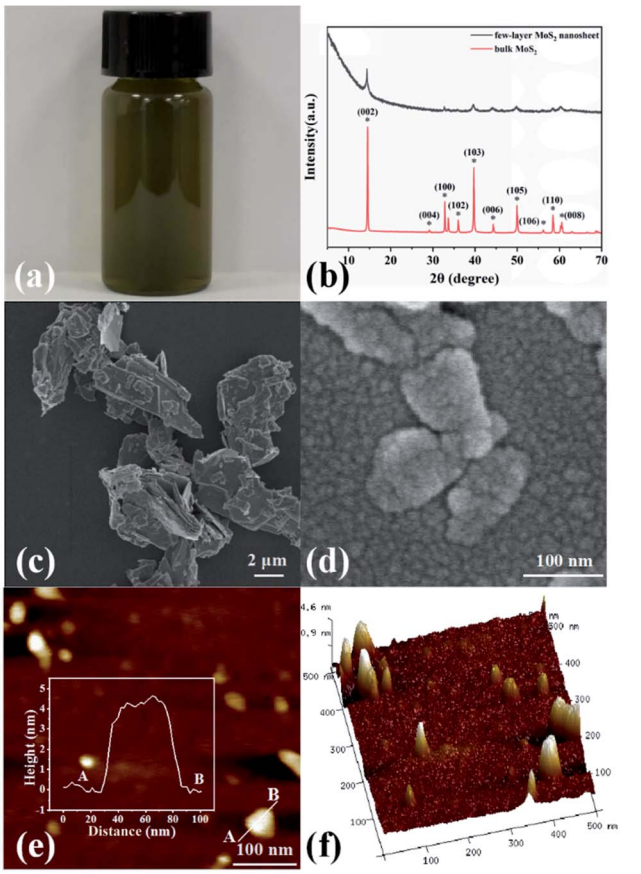

Fig. 2 (a) A dispersion of few-layer MoS_2 nanosheets in water, (b) the XRD patterns of few-layer MoS_2 nanosheets and bulk MoS_2, (c) SEM image of the bulk MoS_2, (d) SEM image of the few-layer MoS_2 nanosheets, (e) AFM images of the few-layer MoS_2 nanosheets, (f) the corresponding three-dimensional image of (e).

the exfoliated MoS_2 nanosheets. The SEM images are shown in Fig. 2(c and d). The SEM images clearly show that the bulk MoS_2 with a diameter of about a few microns and the few-layer MoS_2 nanosheets with the lateral sizes of hundreds of nanometers. This is consistent with the research results of Claudia Backes *et al.* and Arlene O'Neill *et al.*[39,40] AFM was utilized to further analyze the thickness of the MoS_2 nanosheets. As shown in Fig. 2(e and f), the thickness data illustrate that the thickness of the exfoliated MoS_2 nanosheets ranges from 4 nm to 5 nm, which indicate that the thickness of the few-layer nanosheets are less than 10 layers.[38,41] The results demonstrate that few-layer MoS_2 nanosheets with the small lateral size and the thin thickness can be prepared by the simple liquid-based direct exfoliation.

3.2 Electrochemical behavior of different modified electrodes

To study the electrochemical activity of MoS_2, the electrochemical properties of MoS_2 modified electrode were characterized by CV in 1.0 M KCl containing 1.0 mM $[Fe(CN)_6]^{3-/4-}$ in the three-electrode system. As shown in Fig. 3, bare GCE exhibits strong redox peak current, which is due to the good conductivity of bare GCE and the good electron transfer of $[Fe(CN)_6]^{3-/4-}$ on the electrode surface, and the oxidation peak current is 9.595 μA. Compared with bare GCE, the redox peak current of the bulk MoS_2/GCE is slightly increased after being modified with the bulk MoS_2, and the oxidation peak current is 9.891 μA. However, the redox peak current of the MoS_2/GCE increases again after modification with few-layer MoS_2 nanosheets, and the oxidation peak current is 12.146 μA. Compared with bare GCE, the peak current of bulk MoS_2/GCE increases about 3%, while the peak current of few-layer MoS_2/GCE increases about 27%. The results show that the electrochemical activity of MoS_2 can be improved by shear stripping, and effectively promote the electron transfer of $[Fe(CN)_6]^{3-/4-}$ redox pairs on the electrode surface. The different electrochemical activities of few-layer MoS_2 nanosheets and bulk MoS_2 are determined by the anisotropic layered structure of MoS_2. There are obvious differences in electronic structure and electrochemical activity of MoS_2 materials with different layers or sizes.[29,42,43] In principle, the conductivity of MoS_2 is linearly proportional to its thickness, and the thinner the thickness, the greater the conductivity. Studies have shown that when the thickness of MoS_2 decreases from 385 nm to 33 nm, the conductivity increases from 11 Ω^{-1} cm^{-1} to 360 Ω^{-1} cm^{-1}, increasing by more than 30 times.[44] Compared with bulk MoS_2, the prepared few-layer MoS_2 nanosheets have significantly reduced layers, thus showing enhanced conductivity, which is consistent with the results of EIS tests (see ESI, S1†).

3.3 Signal monitoring of DNA immobilization and hybridization

An electrochemical sensing platform based on MoS_2 nanosheets was constructed to explore its ability to detect ctDNA. The fabrication conditions of the electrochemical DNA sensor were optimized (ESI, S2†). MB was used as an electrochemical indicator to study the fixation and hybridization of DNA on this sensing platform.[45,46] The ability of immobilizing cpDNA on the electrode surface was studied first. The DPV signals of MB at working electrodes are displayed in Fig. 4. As shown in Fig. 4, the reduction peak current increases significantly on the MoS_2/GCE working electrode after cpDNA immobilization. Compared with MoS_2/GCE, the peak current increased from 3.496 μA to 4.580 μA. This is due to the special affinity between MB and the free guanine bases exposed out of cpDNA, so a large amount of MB were absorbed at the surface of the cpDNA/MoS_2/GCE working electrode. The results also demonstrated that cpDNA was successfully bounded to the MoS_2/GCE modified electrode surface. The peak currents of bare GCE and cpDNA/GCE were 0.051 μA and 0.230 μA, respectively. Compared with cpDNA/GCE, the peak current value of cpDNA/MoS_2/GCE increased about 20 times, which shows that the MoS_2 is more conducive to adsorb cpDNA. This result proves that few-layer MoS_2 nanosheets not only significantly increased the surface area of the electrode, but also enhanced its electrochemical activity. The larger electrode surface area is conducive to the adsorption of more DNA, and the higher electrochemical activity is conducive

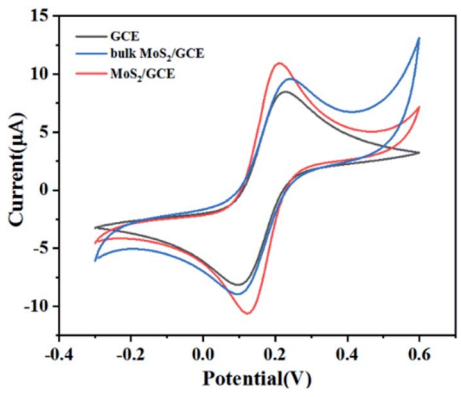

Fig. 3 CV plots obtained at bare GCE, bulk MoS_2/GCE and MoS_2/GCE in 1.0 M KCl containing 1.0 mM $[Fe(CN)_6]^{3-/4-}$. The potential was scanned from 0.6 V to −0.3 V with a scan rate of 100 mV s^{-1}.

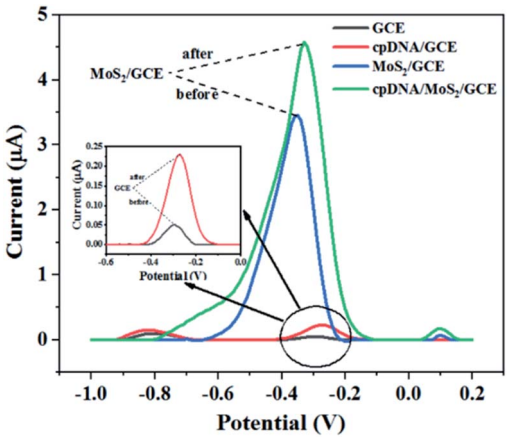

Fig. 4 DPV plots of 2.0×10^{-5} M MB at bare GCE and MoS_2/GCE before and after cpDNA immobilization.

to the transmission of MB on the electrode surface. The joint improvement of the two makes the sensing platform based the MoS_2 nanosheet have a better effect on DNA immobilization.

Next, the specific hybridization capture of ctDNA on few-layer MoS_2 nanosheets sensing platform was studied. As shown in Fig. 5(a), after hybridization with ctDNA of different concentrations, the reduction peak current of MB decreased with the increase of ctDNA concentration. This is because the force between dsDNA and MoS_2 nanosheets becomes weaker after hybridization, and the dsDNA fall off from the electrode surface under the negative potential, which reduces the amount of cpDNA absorbed on the electrode surface and thus decreases the electrochemical signal of MB. The variation trend of the signals indicated that the cpDNA was successfully hybridized with the complementary sequence ctDNA. As shown in Fig. 5(b), the difference (namely ΔI_{pt}) between the reduction peak current value of MB after hybridization and before hybridization is adopted as the measurement signal to study its relationship with the logarithm of ctDNA concentration (namely log C). The results demonstrated that there was a good linear relationship ($R^2 = 0.99805$) between ΔI_{pt} and the ctDNA within the range of 1.0×10^{-7} M to 1.0×10^{-16} M, and the regression equation is ΔI_{pt} (μA) = 0.12939 log C (M) + 2.27808. In addition, the limit of detection (LOD) was 2.5×10^{-18} M, which was calculated by the 3σ method with seven measurements of blank solution. As shown in Table 2, the detection limit of this study is comparable or lower than other electrochemical sensing platforms for the ctDNA detection.

3.4 Specificity

For DNA biosensors, the specificity is also an important characteristic for performance evaluation. To evaluate the specificity of this sensor against DNA sequences, single-base mismatched DNA (1 MT ctDNA), three-base mismatched DNA (3 MT ctDNA), and non-complementary mismatched DNA (nc ctDNA) were investigated. As illustrated in Fig. 6, the signal change is most significant after hybridization with ctDNA, followed by 1 MT ctDNA and 3 MT ctDNA, respectively. And nc ctDNA shows the smallest signal change. Compared with the signal changes after ctDNA hybridization, the signal changes of 1 MT ctDNA, 3 MT ctDNA and nc ctDNA decreased to 80.74%, 57.59% and 25.86%, respectively. The result proves that this sensor exhibits high selectivity towards the ctDNA and could distinguish mismatched and non-complementary DNA sequences.

Table 2 Comparison of the reported methods for ctDNA detection

Method	LOD	Detection range	References
Electrochemistry	2.5 aM	100 aM–100 nM	This work
Electrochemistry	2.4 aM	10 aM–1 pM	47
Electrochemistry	18 aM	100 aM–10 nM	3
LSPR	50 fM	50 fM–3.2 pM	12
Fluorescence	0.3161 pM	1 pM–100 pM	48
Colorimetric	0.32 pM	1 pM–10 nM	49
Electrochemistry	3 pM	5 pM–0.5 nM	2

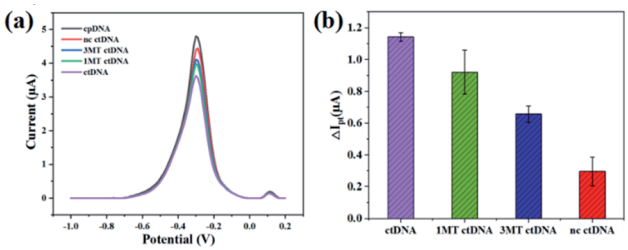

Fig. 6 (a) Comparison of DPV plots hybridization signal changes for cpDNA (1.0×10^{-6} M) modified MoS_2/CPE hybridized with ctDNA, 1 MT DNA, 3 MT DNA, and ncDNA, (b) comparison of hybridization signal changes for cpDNA (1.0×10^{-6} M) modified MoS_2/CPE hybridized with ctDNA, 1 MT DNA, 3 MT DNA, and ncDNA. The detection concentrations of these sequences were all selected as 1.0×10^{-10} M.

3.5 Stability and reproducibility

The stability of the developed DNA electrochemical biosensor was investigated. Five different cpDNA/MoS_2/GCEs were stored at 4 °C for 7 days. The DPV responses to 100 nM ctDNA were shown in Fig. 7(a). The test proved that no apparent change of DPV signals was observed after one week, indicating that the DNA electrochemical biosensor exhibited good stability.

At the same conditions, five cpDNA/MoS_2/GCE modified electrodes were prepared and hybridized with 100 pM ctDNA. The reproducibility of the sensor is evaluated according to the standard deviation of the MB signal values of the modified electrodes. As shown in Fig. 7(b), the result shows that the standard deviation is 8.002%, indicating that the DNA biosensor has excellent reproducibility.

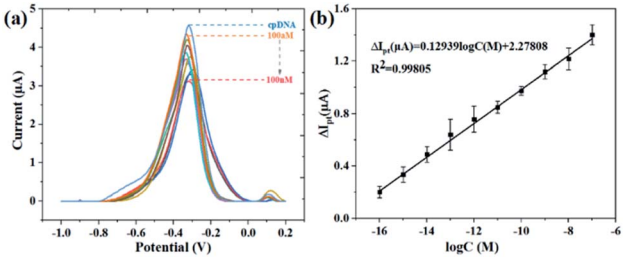

Fig. 5 (a) DPV plots of 2.0×10^{-5} M MB at cpDNA (1.0×10^{-6} M) modified MoS_2/CPE after hybridization with different concentrations of ctDNA, (b) the plot of ΔI_{pt} *versus* the logarithm of ctDNA concentrations.

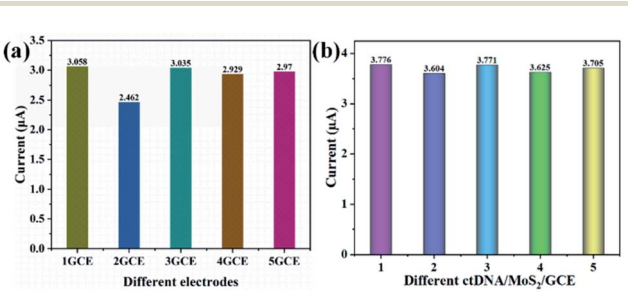

Fig. 7 (a) The DPV signals of 5 different electrodes after 7 days at 4 °C, (b) comparison of DPV plots of five different ctDNA/MoS_2/GCE.

Table 3 Detection of the serum samples by the electrochemical biosensor

Serum	ctDNA added	ctDNA detected	Recovery (%)	RSDs (%)
1	10 pM	9.51 pM, 9.34 pM, 9.28 pM	93.75	4.52
2	100 fM	97.74 fM, 94.25 fM, 91.89 fM	94.21	14.15
3	1 fM	1.01 fM, 0.99 fM, 0.95 fM	98.64	12.77

3.6 Samples analysis

The constructed electrochemical biosensor was applied to explore the practicability for real serum samples. Three different concentrations of ctDNA were spiked into the 10-fold diluted serum samples through the standard addition method. As shown in Table 3, the experiments results indicated that the recoveries ranged from 93.75% to 98.64% with a relative standard deviations (RSDs) of less than 15%. This sample experiment demonstrated the feasibility of the proposed electrochemical DNA detection platform for detecting targets in real DNA samples.

4 Conclusions

In summary, the bulk MoS_2 powder was separated into few-layer MoS_2 nanosheets in an aqueous sodium cholate solution using a blender, which is simple to operate and allows mass production. Moreover, the prepared few-layer MoS_2 nanosheets have high electrochemical activity. The few-layer MoS_2 nanosheets was modified on the electrode surface and MB was introduced as signal molecule to develop an electrochemical biosensor for detecting tumor marker ctDNA. The experimental results demonstrated that this biosensor had significant superiority for ctDNA detection, which achieved ultralow detection limit of 2.5×10^{-18} M and had a good linearity during the ctDNA concentration ranging from 1.0×10^{-7} M to 1.0×10^{-16} M. In addition, this sensor platform has excellent sensitivity, specificity and stability, providing an alternative approach for ctDNA detection.

Author contributions

Zhilian Cui: investigation, validation, writing – original draft. Dujuan Li: conceptualization, methodology, writing – review & editing. Weihuang Yang: writing – review & editing. Kai Fan: writing – review & editing. Hongying Liu: resources. Fei Wen: resources. Lili Li: resources. Linxi Dong: resources. Gaofeng Wang: supervision, funding acquisition. Wei Wu: resources.

Conflicts of interest

There are no conflicts to declare.

Acknowledgements

We appreciate the financial support from the National Natural Science Foundation of China (31201367), National Key R&D Program Grant (No. 2018YFE0120000), and NSFC Key Grant (62141409).

References

1 S. Avanzini, D. M. Kurtz, J. J. Chabon, E. J. Moding, S. S. Hori, S. S. Gambhir, A. A. Alizadeh, M. Diehn and J. G. Reiter, *Sci. Adv.*, 2020, **6**, eabc4308.
2 Y. Huang, M. Tao, S. Luo, Y. Zhang, B. Situ, X. Ye, P. Chen, X. Jiang, Q. Wang and L. Zheng, *Anal. Chim. Acta*, 2020, **1107**, 40–47.
3 W. Zhang, Z. Dai, X. Liu and J. Yang, *Biosens. Bioelectron.*, 2018, **105**, 116–120.
4 D. Li, H. Chen, K. Fan, V. Labunov, S. Lazarouk, X. Yue, C. Liu, X. Yang, L. Dong and G. Wang, *Biosens. Bioelectron.*, 2021, **181**, 113147.
5 H. A. Loomans-Kropp and A. Umar, *npj Precis. Oncol.*, 2019, **3**, 1–8.
6 C. Cai, Z. Guo, Y. Cao, W. Zhang and Y. Chen, *Nanotheranostics*, 2018, **2**, 12.
7 B. Jimenez Rodriguez, G. Diaz Cordoba, A. Garrido Aranda, M. Álvarez, L. Vicioso, C. Llacer Perez, C. Hernando, B. Bermejo, A. Julve Parreno and A. Lluch, *J. Clin. Med.*, 2019, **8**, 1183.
8 H. Liao and H. Li, *Cancer Manage. Res.*, 2020, **12**, 3547.
9 N. Papadopoulos, *Tumor Liquid Biopsies*, 2020, pp. 163–180.
10 C.-H. Marquette, J. Boutros, J. Benzaquen, M. Ferreira, J. Pastre, C. Pison, B. Padovani, F. Bettayeb, V. Fallet and N. Guibert, *Lancet Respir. Med.*, 2020, **8**, 709–716.
11 H. Chang, Y. Zhang, F. Yang, C. Wang and H. Dong, *Front. Chem.*, 2018, **6**, 530.
12 A. H. Nguyen and S. J. Sim, *Biosens. Bioelectron.*, 2015, **67**, 443–449.
13 A. E. Rodda, B. J. Parker, A. Spencer and S. R. Corrie, *ACS Sens.*, 2018, **3**, 540–560.
14 J. Das, I. Ivanov, L. Montermini, J. Rak, E. H. Sargent and S. O. Kelley, *Nat. Chem.*, 2015, **7**, 569–575.
15 X. Wang, F. Nan, J. Zhao, T. Yang, T. Ge and K. Jiao, *Biosens. Bioelectron.*, 2015, **64**, 386–391.
16 V. Yadav, S. Roy, P. Singh, Z. Khan and A. Jaiswal, *Small*, 2019, **15**, 1803706.
17 L. Lan, Y. Yao, J. Ping and Y. Ying, *Sens. Actuators, B*, 2019, **290**, 565–572.
18 B. L. Li, H. L. Zou, L. Lu, Y. Yang, J. L. Lei, H. Q. Luo and N. B. Li, *Adv. Funct. Mater.*, 2015, **25**, 3541–3550.
19 J. Huang, L. Ye, X. Gao, H. Li, J. Xu and Z. Li, *J. Mater. Chem. B*, 2015, **3**, 2395–2401.

20 L. Xiao, L. Xu, C. Gao, Y. Zhang, Q. Yao and G.-J. Zhang, *Sensors*, 2016, **16**, 1561.
21 S. Dutta, A. D. Chowdhury, S. Biswas, E. Y. Park, N. Agnihotri, A. De and S. De, *Biochem. Eng. J.*, 2018, **140**, 130–139.
22 Y. Zhou, F. Li, H. Wu, Y. Chen, H. Yin, S. Ai and J. Wang, *Sens. Actuators, B*, 2019, **296**, 126664.
23 M. Sadeghi, M. Jahanshahi and H. Javadian, *Microchem. J.*, 2020, **152**, 104315.
24 L. Lan, D. Chen, Y. Yao, X. Peng, J. Wu, Y. Li, J. Ping and Y. Ying, *ACS Appl. Mater. Interfaces*, 2018, **10**, 42009–42017.
25 L. Zhao, D. Kong, Z. Wu, G. Liu, Y. Gao, X. Yan, F. Liu, X. Liu, C. Wang and J. Cui, *Microchem. J.*, 2020, **155**, 104675.
26 W. Zhang, J. Yang and D. Wu, *J. Electrochem. Soc.*, 2020, **167**, 027501.
27 L. Zhao, J. Wang, D. Su, Y. Zhang, H. Lu, X. Yan, J. Bai, Y. Gao and G. Lu, *Nanoscale*, 2020, **12**, 19420–19428.
28 C. Zhu, Z. Zeng, H. Li, F. Li, C. Fan and H. Zhang, *J. Am. Chem. Soc.*, 2013, **135**, 5998–6001.
29 Z. Meng, R. M. Stolz, L. Mendecki and K. A. Mirica, *Chem. Rev.*, 2019, **119**, 478–598.
30 Y. Chu, B. Cai, Y. Ma, M. Zhao, Z. Ye and J. Huang, *RSC Adv.*, 2016, **6**, 22673–22678.
31 L. Lan, Y. Yao, J. Ping and Y. Ying, *ACS Appl. Mater. Interfaces*, 2017, **9**, 23287–23301.
32 M. Kukkar, G. C. Mohanta, S. K. Tuteja, P. Kumar, A. S. Bhadwal, P. Samaddar, K.-H. Kim and A. Deep, *Biosens. Bioelectron.*, 2018, **107**, 244–258.
33 T. Yang, Q. Guan, X. Guo, L. Meng, M. Du and K. Jiao, *Anal. Chem.*, 2013, **85**, 1358–1366.
34 G. Zhang, Y. Li, X. Xiao, Y. Shan, Y. Bai, H.-G. Xue, H. Pang, Z. Tian and Q. Xu, *Nano Lett.*, 2021, **21**, 3016–3025.
35 W. Li, X. Guo, P. Geng, M. Du, Q. Jing, X. Chen, G. Zhang, H. Li, Q. Xu and P. Braunstein, *Adv. Mater.*, 2021, **33**, 2105163.
36 P. Geng, L. Wang, M. Du, Y. Bai, W. Li, Y. Liu, S. Chen, P. Braunstein, Q. Xu and H. Pang, *Adv. Mater.*, 2022, **34**, 2107836.
37 H. Duan, T. Wang, X. Wu, Z. Su, J. Zhuang, S. Liu, R. Zhu, C. Chen and H. Pang, *Chin. Chem. Lett.*, 2020, **31**, 2330–2332.
38 E. Varrla, C. Backes, K. R. Paton, A. Harvey, Z. Gholamvand, J. McCauley and J. N. Coleman, *Chem. Mater.*, 2015, **27**, 1129–1139.
39 C. Backes, R. J. Smith, N. McEvoy, N. C. Berner, D. McCloskey, H. C. Nerl, A. O'Neill, P. J. King, T. Higgins and D. Hanlon, *Nat. Commun.*, 2014, **5**, 1–10.
40 A. O'Neill, U. Khan and J. N. Coleman, *Chem. Mater.*, 2012, **24**, 2414–2421.
41 K. R. Paton, E. Varrla, C. Backes, R. J. Smith, U. Khan, A. O'Neill, C. Boland, M. Lotya, O. M. Istrate and P. King, *Nat. Mater.*, 2014, **13**, 624–630.
42 C. Anichini, W. Czepa, D. Pakulski, A. Aliprandi, A. Ciesielski and P. Samorì, *Chem. Soc. Rev.*, 2018, **47**, 4860–4908.
43 H. Duan, Z. Zhao, J. Lu, W. Hu, Y. Zhang, S. Li, M. Zhang, R. Zhu and H. Pang, *ACS Appl. Mater. Interfaces*, 2021, **13**, 33083–33090.
44 M. Siao, W. Shen, R. Chen, Z. Chang, M. Shih, Y. Chiu and C.-M. Cheng, *Nat. Commun.*, 2018, **9**, 1–12.
45 S. Su, Q. Hao, Z. Yan, R. Dong, R. Yang, D. Zhu, J. Chao, Y. Zhou and L. Wang, *Microchim. Acta*, 2019, **186**, 1–11.
46 F. Li, J. Peng, Q. Zheng, X. Guo, H. Tang and S. Yao, *Anal. Chem.*, 2015, **87**, 4806–4813.
47 H.-F. Wang, R.-N. Ma, F. Sun, L.-P. Jia, W. Zhang, L. Shang, Q.-W. Xue, W.-L. Jia and H.-S. Wang, *Biosens. Bioelectron.*, 2018, **122**, 224–230.
48 C. Chen, R. He, Z. Zhang and Y. Chen, *Analyst*, 2020, **145**, 7603–7608.
49 X. Mao, S. Pan, D. Zhou, X. He and Y. Zhang, *Sens. Actuators, B*, 2019, **285**, 385–390.

